

## Article

# Assessment and Non-Destructive Evaluation of the Influence of Residual Solvent on a Two-Part Epoxy-Based Adhesive Using Ultrasonics

Gonzalo Seisdedos <sup>1</sup>, Edgar Viamontes <sup>1</sup>, Eduardo Salazar <sup>1</sup>, Mariana Ontiveros <sup>1</sup>, Cristian Pantea <sup>2</sup>, Eric S. Davis <sup>2</sup>, Tommy Rockward <sup>2</sup>, Dwayne McDaniel <sup>1</sup> and Benjamin Boesl <sup>1,\*</sup>

<sup>1</sup> Mechanical and Materials Engineering Department, Florida International University, Miami, FL 33199, USA

<sup>2</sup> Materials Physics and Applications (MPA-11), Los Alamos National Laboratory, Los Alamos, NM 87545, USA

\* Correspondence: bboesl@fiu.edu

**Featured Application:** Non-destructive evaluation of polymer curing using ultrasonics.

**Abstract:** Polymers are increasingly being used in higher demanding applications due to their ability to tailor the properties of structures while allowing for a weight and cost reduction. Solvents play an important role in the manufacture of polymeric structures since they allow for a reduction in the polymer's viscosity or assist with the dispersion of fillers into the polymer matrix. However, the incorrect removal of the solvent affects both the physical and chemical properties of polymeric materials. The presence of residual solvent can also negatively affect the curing kinetics and the final quality of polymers. Destructive testing is mainly performed to characterize the properties of these materials. However, this type of testing involves using lab-type equipment that cannot be taken in-field to perform in situ testing and requires a specific sample preparation. Here, a method is presented to non-destructively evaluate the curing process and final viscoelastic properties of polymeric materials using ultrasonics. In this study, changes in longitudinal sound speed were detected during the curing of an aerospace epoxy adhesive as a result of variations in polymer chemistry. To simulate the presence of residual solvent, samples containing different weight percentages of isopropyl alcohol were manufactured and tested using ultrasonics. Thermogravimetric analysis was used to show changes in the decomposition of the adhesive due to the presence of IPA within the polymer structure. Adding 2, 4, and 6 wt.% of IPA decreased the adhesive's lap shear strength by 40, 58, and 71%, respectively. Ultrasonics were used to show how the solvent influenced the curing process and the final sound speed of the adhesive. Young's modulus and Poisson's ratio were determined using both the longitudinal and shear sound speeds of the adhesive. Using ultrasonics has the potential to non-invasively characterize the quality of polymers in both an in-field and manufacturing settings, ensuring their reliability during use in demanding applications.

**Keywords:** acoustics; ultrasonics; composites; adhesive bonding; non-destructive testing; TGA; lap shear; polymers; cure kinetics; modeling; residual solvent; elastic moduli; FTIR



**Citation:** Seisdedos, G.; Viamontes, E.; Salazar, E.; Ontiveros, M.; Pantea, C.; Davis, E.S.; Rockward, T.; McDaniel, D.; Boesl, B. Assessment and Non-Destructive Evaluation of the Influence of Residual Solvent on a Two-Part Epoxy-Based Adhesive Using Ultrasonics. *Appl. Sci.* **2023**, *13*, 3883. <https://doi.org/10.3390/app13063883>

Academic Editor: Ana Martins Amaro

Received: 22 February 2023

Revised: 15 March 2023

Accepted: 16 March 2023

Published: 18 March 2023



**Copyright:** © 2023 by the authors. Licensee MDPI, Basel, Switzerland. This article is an open access article distributed under the terms and conditions of the Creative Commons Attribution (CC BY) license (<https://creativecommons.org/licenses/by/4.0/>).

## 1. Introduction

The manufacturing conditions of polymeric materials are critical since they determine the resulting polymer structure, and as an outcome, its final properties and performance characteristics [1–4]. Therefore, it is important to monitor polymers during the fabrication process to enhance our understanding of their relationship to the final quality of the manufactured parts. Ensuring polymers have the required characteristics will help improve their reliability when used in primary structures in fields such as aerospace, automotive, biomedical, electrochemical, etc.

When manufacturing polymers, solvents play an important role since they allow for a reduction in the polymer's viscosity during a coating process or assist with the dispersion

of fillers into the polymer matrix [5–7]. This inevitably raises the concern of improperly removing the solvent from the polymer before obtaining its final structure. It has been shown that the incorrect removal of the solvent affects both the physical and chemical properties of polymers [8–11]. For example, J. Trinidad et al. showed that the presence of solvent in sodium dodecyl sulfate decorated graphene hybrid electrically conductive adhesives significantly decreased their lap shear strength due to the presence of voids and bubble formation [12]. N. Othman et al. experienced a decrease in tensile strength and hardness of 17 and 9%, respectively, when adding 16 wt.% of acetone in an epoxy resin [6]. Their study also showed that having this amount of acetone caused a decline in the epoxy's adhesion strength from 13 MPa to 4.9 MPa, which signifies a reduction of ~62%. In addition, K. Qiu et al. demonstrated that residual solvent content in an epoxy resin affected its curing mechanics and decreased its crosslinking density. This lowered the glass transition temperature ( $T_g$ ) of the resin by ~8.5 °C when they added 5 wt.% of cellular nanocrystals as a filler due to a decrease in the homogeneity of the material [13]. Since having residual solvent can negatively affect the properties of a polymeric material, it is important to have a precise evaluation method to determine if the solvent is present in the final structure.

Destructive testing, which involves using lab-type instrumentation that requires a specific sample preparation and geometry, is mainly performed to characterize the mechanical properties of materials [14–21]. It has also been used to characterize the curing kinetics of polymeric materials. Tests include dynamic mechanical analysis (DMA), differential scanning calorimetry (DSC), thermogravimetric analysis (TGA), tensile testing, lap shear testing, etc. However, this type of equipment cannot be taken in-field to perform in situ testing. Therefore, it has become essential to develop a non-destructive in situ method to evaluate the degree of reaction and the viscoelastic properties of polymers during curing and after they have been manufactured [22,23].

Acoustics, consisting of the propagation of sound waves, have been used as a non-destructive evaluation method for different types of materials such as metals [24–26], ceramics [27,28], and polymers [22,29], due to their accuracy and sensitivity. Ultrasonics, which involve the use of acoustic waves at high frequencies (20 kHz–100 MHz), can be used to detect small changes in adiabatic moduli with high precision. Therefore, ultrasonics can be implemented to evaluate phase transitions during curing and the physical properties of materials [22,30]. For example, the ultrasonic pulse-echo method can be implemented to measure the sound speed of a material with a short pulse of ultrasound generated by a transducer, from which elastic constants of the material can be determined [30]. F. Lionetto et al. used ultrasonics to monitor the cure state of thermosetting resins and showed how ultrasonic wave propagation was more sensitive to variations in moduli during the vitrification stage of the curing process compared to DSC [31]. This method has also been used to non-destructively evaluate the curing mechanics of epoxy resins at different temperatures [22,31,32]. However, a deeper understanding of the use of ultrasonics as a non-destructive method is needed to effectively understand the curing mechanics of resins and adhesives under different parameters that can affect the quality of the final product.

As an example, in the aerospace industry, epoxy and film adhesives are used to substitute mechanical fasteners for joining carbon fiber composites. This methodology has been proposed as a result of an adhesive bond's potential for increased strength, weight reduction, and improved stress distribution [33–35]. On the other hand, the Federal Aviation Administration (FAA) is concerned about the performance of adhesive bonds after aging during their life cycle [36]. In addition, failures associated with weak bonds, bondline voids, and contamination remain critical issues in today's adhesion community [37]. Manufacturing parameters, such as temperature and pressure, are difficult to precisely control and unwanted fluctuations can have an impact on the curing process and final product [38]. In addition, the usage of a mold release or other chemicals throughout the manufacturing process can lead to potential contamination and reduction in performance [39,40]. As men-

tioned, the presence of residual solvent on an epoxy adhesive can considerably decrease its adhesive strength [6].

The focus of this paper is to detect changes in sound speed in an aerospace epoxy adhesive during the curing process as a result of residual solvent concentration. In this study, varying amounts of isopropyl alcohol (IPA) were added into the adhesive to simulate trapped solvent. Since the addition of IPA affects the crosslinking density and mobility of the adhesive, TGA was performed to analyze the decomposition of each of the sample types and to confirm the presence of different weight percentages of IPA in the adhesive samples. Fourier transform infrared (FTIR) spectroscopy was performed to investigate the effects in the chemical structure of the samples as a function of solvent concentration. Lap shear testing was used to evaluate the effects of IPA on the mechanical and adhesion properties of the adhesive under a shear load. We hypothesize that the sending and receiving of ultrasonic waves has the ability to detect the presence of this solvent and to determine how it influences the curing process of the adhesive. This curing process was modeled to better understand how variations in trapped solvent affect the curing mechanics of the material. Comprehending these effects can improve future techniques designed to use ultrasonics as an in situ, non-destructive quality control method during the manufacturing process. In addition, measuring the sound speed of fully cured samples that have been properly manufactured can serve as an in-field quality control method during the lifetime of polymeric materials.

## 2. Materials and Methods

In this study, a two-part epoxy adhesive (EC 2615 B/A, 3M) was selected and used as a representative material. This adhesive is a two-part DEGBA-based resin with an amine hardener. A 2:1 resin-(part B)-to-hardener-(part A) ratio was used as recommended by the manufacturer. To simulate the effect of the trapped solvent, adhesive samples with 2, 4, and 6 weight percentages (wt.%) of isopropyl alcohol (IPA) were manufactured. IPA was selected since it is a commonly used solvent for manufacturing polymeric materials and structures [41–44]. The curing and testing took place in a monitored laboratory environment at room temperature ( $\sim 23 \pm 2$  °C) and  $\sim 44 \pm 2.5\%$  relative humidity.

### 2.1. Thermal Analysis (TGA)

Thermal analysis was performed using a Q600 SDT (TA Instruments, New Castle, DE, USA) on fully cured adhesive samples containing 0, 2, 4, and 6 wt.% IPA. The tests were run from room temperature ( $\sim 23$  °C) to 450 °C at a heating rate of 5 °C/min. Argon gas was used as a purge gas. The weight of the samples ranged between 9 and 9.5 µg.

### 2.2. Fourier Transform Infrared (FTIR) Spectroscopy

FTIR spectroscopy was performed on a Nicolet iS50 spectrometer (Thermo Fisher Scientific, Waltham, MA, USA) from 3600 to 400  $\text{cm}^{-1}$  with a resolution of 0.482  $\text{cm}^{-1}$ . A DTGS KBr detector and OMNIC software were utilized. Sixteen scans were used and the spectra were graphed on absorbance mode. The lens was cleaned using ethanol and a background scan was completed before testing each sample. In addition to the samples analyzed by TGA, FTIR spectroscopy was also performed on the IPA used to simulate the residual solvent.

### 2.3. Single Lap Shear

Lap shear testing was performed on carbon fiber composite samples bonded using adhesive manufactured with 0, 2, 4, and 6 wt.% IPA. The ASTM D5868-01 [45] standard was followed for the manufacture and testing of the lap shear samples. Four specimens per sample type were manufactured and tested. An autoclave (American Autoclave Co., Jasper, TX, USA) was used to cure the prepreg layup at a temperature of 177 °C and a pressure of 30 psi for 1 hour. A polyester peel ply was placed on both sides of the prepreg layups in order to prepare the surface for bonding. The lap shear specimens were cut to a size of

25.4 mm by 177.8 mm with a bonded area of 25.4 mm by 25.4 mm. A tensile tester from MTS (Criterion Model 43) was used to test the samples with a loading rate of 13 mm/min.

#### 2.4. Ultrasonics: Cure Process

Ultrasonics were utilized to non-destructively measure the sound speed of the adhesive during its curing process. To perform this testing during the adhesive's curing process, the adhesive was first mixed and then placed in a PLA 3D printed mold. The mold had dimensions of 20 mm in height, 22 mm in width, and 12.5 mm in thickness. The mold's wall thickness was 1.5 mm, except for the locations where the transducers were placed, which had a thickness of 0.5 mm. A function generator (AFG31052; Tektronix, Beaverton, OR, USA) was utilized to generate a sine burst of 500 kHz at 10 volts peak-to-peak. This frequency was selected after observation over a range of frequencies as it produced the highest output signal for this particular adhesive material. A Tukey window with a cosine fraction,  $r$ , of 0.4 was used to taper the input function consisting of five cycles [46]. The burst was transmitted and detected by transducers placed on each side of the sample. Transducers (V133-RM and V154-RM, Olympus, Center Valley, PA, USA) of 2.25 MHz were used for evaluating the longitudinal and shear sound speeds, respectively. An ultrasonic couplant (Echo Ultrasonics, Bellingham, WA, USA) was used to ensure proper contact between the sample and the transducers. The resulting waveforms were recorded every two minutes using an oscilloscope (MDO32; Tektronix, Beaverton, OR, USA). Figure 1a shows a diagram of the ultrasonics setup, where the sample is depicted in blue and the transducers, in green. The output waveforms were then used along with the excitation waveform to calculate the sound travel time across the sample utilizing the cross-correlation method [30]. It is important to mention that the delays introduced to this travel time by the transducers and the PLA mold, where the adhesive was placed, were accounted for prior to using Equation (1) to calculate the sound speed in the material:

$$c = \frac{d}{t} \quad (1)$$

where  $d$  is the thickness of the sample and  $t$  is the sound travel time. The law of propagation of uncertainty was used to obtain the error associated with the velocity calculations [47]. This method accounts for the uncertainty associated with the resolution of the oscilloscope to plot the output waveforms (9 ns), which were used to obtain the sound travel time, and the uncertainty associated with the digital micrometer which was used to evaluate the thickness of the sample (0.01 mm).

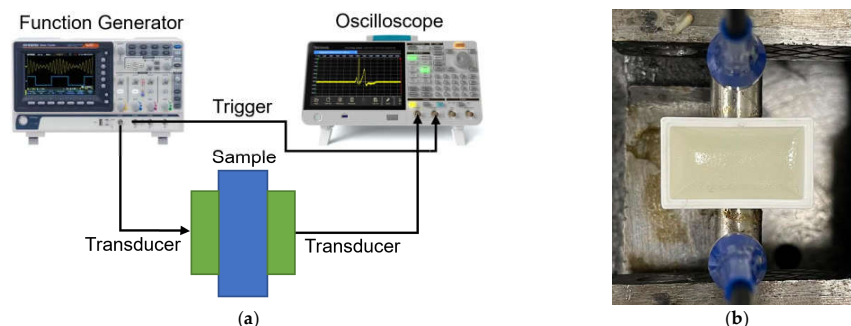


**Figure 1.** (a) Diagram of the ultrasonics instrumentation and sample setup; (b) picture of an adhesive sample while being tested during curing.

#### 2.5. Cure Process Modeling

The Hill equation was used to model the curing process for each of the samples. This was used to help to better understand how variations in trapped solvent affected the curing mechanics of the adhesive and to allow for future predictions of material quality. The

degree of conversion,  $\alpha(t)$ , ranges from 0 to 1 and can be expressed using the Hill equation as shown in Equation (2) [48]:

$$\alpha = 1 - \frac{1}{\left(\frac{t}{\tau}\right)^\theta} \quad (2)$$

where  $t$  is the curing time in seconds,  $\theta$  is the shape parameter constant, and  $\tau$  is the time constant defined as  $\tau = \theta/k$ , where  $k$  is the rate constant. The time constant  $\tau$  is an important parameter of the distribution since it represents when the degree of conversion  $\alpha = 0.5$ . A generalized reduced gradient (GRG) algorithm was used to minimize the sum of the errors squared between the experimental and modeled data by fitting different  $\theta$  and  $k$  parameters.

### 2.6. Ultrasonics: Elastic Properties

The elastic properties of an isotropic material can be obtained using ultrasonics if its density, longitudinal speed, and shear speed are known [22,49]. The density of a baseline sample (2:1 resin-to-hardener ratio) was obtained using a pycnometer from Micromeritics (AccuPyc II 1340). Using the ultrasonics setup previously mentioned in this section along with the cross-correlation method, a frequency sweep similar to the one performed by C. Pantea et al. [30] was used to accurately determine the longitudinal and shear sound travel times in the adhesive sample. For the longitudinal travel time, a frequency sweep from 0.9 to 2.3 MHz with a 0.1 MHz step was used, while for the shear travel time, a range from 0.5 to 1 MHz was used with the same step size. Different frequency ranges were used to obtain the longitudinal and shear travel times since a minimum amount of signal was required to perform an accurate measurement, but the magnitude of the output signal varied for each frequency and wave type. For homogenous isotropic materials, Equations (3) and (4) can be used to determine Young's modulus and Poisson's ratio, respectively [50]:

$$E = \rho c_s^2 \left( \frac{3c_l^2 - 4c_s^2}{c_l^2 - c_s^2} \right) \quad (3)$$

$$v = \frac{c_l^2 - 2c_s^2}{2c_l^2 - 2c_s^2} \quad (4)$$

where  $\rho$  is the density of the material,  $c_l$  is the longitudinal speed in,  $c_s$  is the shear speed,  $E$  is the Young's modulus, and  $v$  is the Poisson's ratio.

To compare it with destructive testing, the Young's modulus of the adhesive was also determined using tensile testing. Three tensile testing dogbone samples were manufactured and tested following ASTM D638-03 [51]. The MTS tensile tester previously mentioned was used to test the dogbone samples at a loading rate of 5 mm/min. The size of sample type I in the standard was adapted to reduce the amount of material volume used per sample. The dimensions were reduced to have a total length of 87 mm while the thickness was 4.68 mm. The width at the center of the sample and at the grips was 6.84 and 10 mm, respectively. The samples were manufactured by casting the adhesive into a PLA 3D printed mold.

## 3. Results

### 3.1. Thermal Analysis

TGA was performed on the adhesive samples to analyze their thermal decomposition to demonstrate differences in their chemical composition due to the presence of IPA in the studied samples. It can be observed in Figure 2a how the samples containing IPA started decomposing earlier than the baseline sample (0% IPA) at  $\sim 100$  °C, which is most likely due to the solvent causing a decrease in their crosslinking density and an increase in their chain mobility. Similar behavior was observed by N. Othman et al. with 16 wt.% of acetone in an epoxy resin [6]. Figure 2b, which is an augmented version of what is located inside the dashed rectangle in Figure 2a, demonstrates how this behavior was more accentuated with increasing IPA content. All the samples experienced a sharp decrease in weight percentages

with a similar onset temperature ( $\sim 320$  °C). The adhesive samples containing 0, 2, 4, and 6 wt.% of IPA experienced a weight loss of around 2.3, 3.8, 4.8, and 6.2%, respectively.

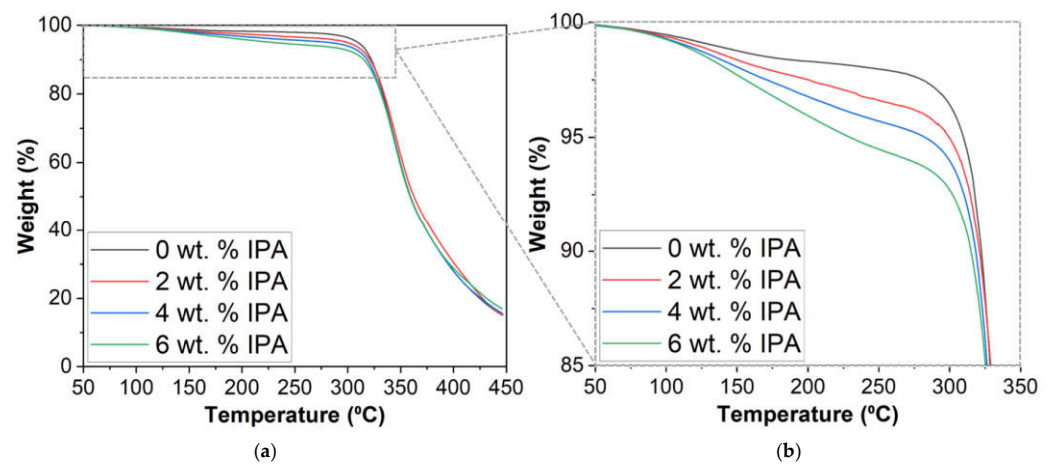


**Figure 2.** TGA of adhesive samples containing 0, 2, 4, and 6 wt.% of IPA (a) from 0 to 450 °C; (b) from 50 to 350 °C located inside the dashed rectangle of Figure 2a.

### 3.2. Fourier Transform Infrared (FTIR) Spectroscopy

The FTIR spectra for the analyzed samples are shown in Figure 3. The region between 400 and 1600  $\text{cm}^{-1}$  contains the fingerprint region for these materials and special attention was given to the area between 900 and 1000  $\text{cm}^{-1}$  since one of the characteristic peaks of IPA is located at 950  $\text{cm}^{-1}$  [52]. As observed in the spectra of the adhesive samples containing IPA, a peak is present at that wavenumber, indicating the presence of this solvent within the adhesive's structure. On the other hand, this peak is not visible in the adhesive sample that contained no IPA. Having solvent within the structure of the adhesive may have altered the crosslinking process and caused a reduction in the molecular weight of some of the polymer chains [53].

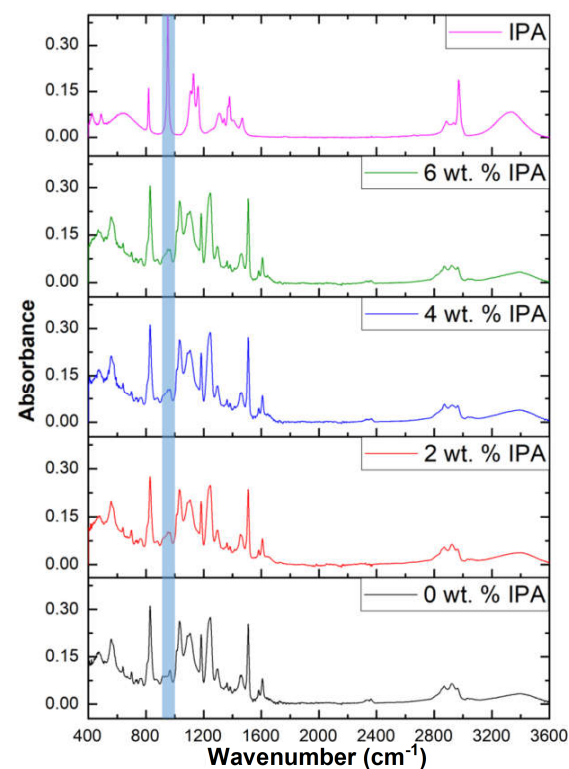


**Figure 3.** FTIR spectra for IPA and for cured adhesive samples containing 0, 2, 4, 6 wt.% IPA.

### 3.3. Single Lap Shear

The resultant peak lap shear stresses for each of the specimens are recorded in Table 1. The average lap shear stress for the samples without IPA content was 21.18 MPa, which is consistent with what has been previously observed [54]. The samples containing IPA experienced a considerable reduction in strength. The average lap shear stresses for the samples containing 2, 4, and 6 wt.% were 12.62 (−40.42%), 8.92 (−57.88%), and 6.07 MPa (−71.35%), respectively. These results show that even the presence of a small quantity of trapped solvent in the two-part epoxy adhesive considerably influenced its adhesion properties to the point where catastrophic failure could occur.

**Table 1.** Maximum lap shear stress of adhesive samples containing 0, 2, 4, and 6 wt.% IPA.

Sample Type/Sample	Peak Lap Shear Stress (MPa)				Std. Dev. (MPa)	Avg. Stress (MPa)
	1	2	3	4		
0 wt.% IPA	21.37	17.63	25.55	-	3.46	21.18
2 wt.% IPA	13.02	15.29	11.21	10.96	2.00	12.62 (−40.42%)
4 wt.% IPA	8.81	6.96	10.73	8.18	1.68	8.92 (−57.88%)
6 wt.% IPA	6.65	6.91	5.16	5.56	0.84	6.07 (−71.34%)

The load–displacement curves of the specimens #1 in Table 1 for each sample type are shown in Figure 4a. The presence of IPA not only lowered the maximum load, but it also decreased the displacement required for failure to occur. This displacement ranged from 3.26 mm for the sample without IPA content down to 0.88 mm for the sample containing 6 wt.% IPA. As seen in Figure 4b, all the sample types experienced the same failure mechanism where the samples failed at the adhesive–substrate interface. No visual differences on the failure surfaces between each sample type were observed, which accentuates the need for a non-destructive evaluation method for this type of material.

**Table 2.** Rate constant  $k$  and shape parameter  $\theta$  of the Hill equation model for each sample type.

Sample	$k (\times 10^{-4})$	$\theta$	Sum of Error Squared
0 wt.% IPA	4.63	1.37	0.0352
2 wt.% IPA	3.48	1.46	0.0262
4 wt.% IPA	2.66	1.48	0.0224
6 wt.% IPA	2.34	1.35	0.0244

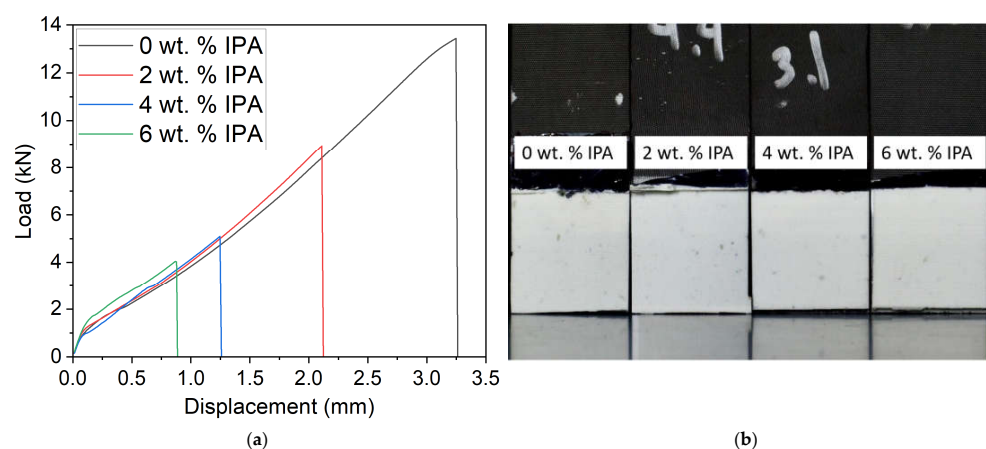


**Figure 4.** (a) Load–displacement curves of the specimens #1 in Table 2 for each sample type; (b) failure surfaces for the specimens represented in the load–displacement curves in Figure 4a.

### 3.4. Monitoring the Sound Travel Speed during the Curing Process Using Ultrasonics

The longitudinal sound speed was first evaluated in three adhesive baseline samples during their curing process. The samples were fabricated and tested simultaneously to determine the repeatability of the analysis technique. It can be observed in Figure 5 that the sound speed of the three samples behaved very similarly, where a sharp increase in sound speed occurs during the first four hours of curing, followed by a convergence until the sample is fully cured. After four days of curing, the final sound speeds for the first, second, and third baseline samples were 2319 ( $\pm 47$ ) m/s, 2317 ( $\pm 46$ ) m/s, and 2320 ( $\pm 47$ ) m/s, respectively. The difference between the samples with the highest and lowest sound speeds was  $\sim 0.13\%$ .

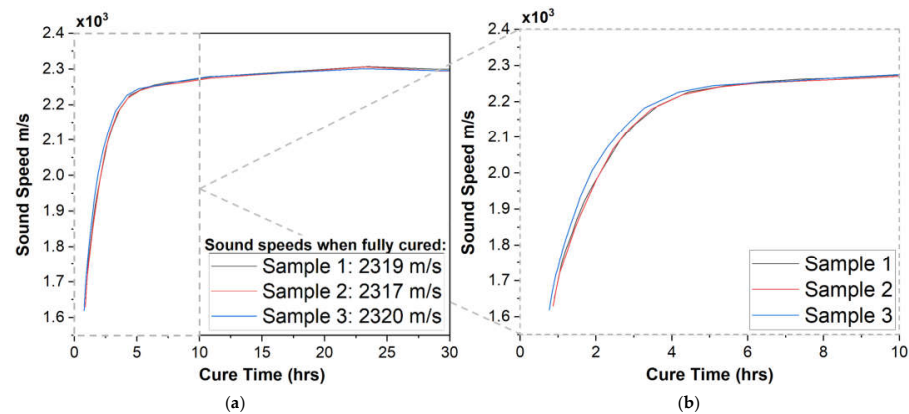


**Figure 5.** Sound speed with respect to cure time of three adhesive baseline samples during (a) the first 30 curing hours; (b) the first 10 curing hours located in the dashed rectangle in Figure 5a.

After adding 2, 4, and 6 wt.% of IPA to the adhesive samples to simulate a trapped solvent, their sound speed was also evaluated during the curing process. Figure 6 shows how, unlike as previously seen with the baseline samples, the curing process differs for each sample. The sound speed of the sample with no IPA content started converging at a lower cure time, while adding IPA delayed the convergence process. To give some perspective, the curve onset of the sample with 0 wt.% IPA occurred at 1.89 curing hours, while the onset for the samples with 2, 4, and 6 wt.% IPA occurred at 2.77, 3.34, and 3.99 curing hours, respectively. This shows a difference of approximately 2.1 h between the baseline sample without IPA and the sample containing 6 wt.% IPA. In addition, the sound speeds after four curing days for the samples with 0, 2, 4, and 6 wt.% of IPA were 2322 ( $\pm 47$ ), 2369 ( $\pm 49$ ), 2354 ( $\pm 48$ ), and 2351 ( $\pm 48$ ) m/s, respectively. This shows how IPA content not only affected the curing mechanics of the adhesive, but also its final sound speed.

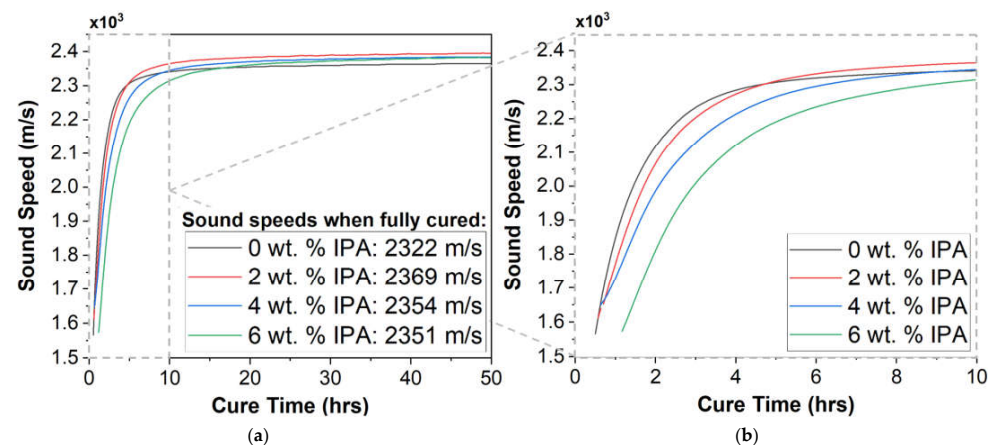


**Figure 6.** Sound speed with respect to cure time of adhesive samples containing 0, 2, 4, and 6 wt.% of IPA during (a) the first 30 curing hours; (b) the first 10 curing hours located in the dashed rectangle in Figure 6a.

### 3.5. Cure Modeling Using the Hill Equation

To numerically understand how trapped solvent affected the cure kinetics of the adhesive, the Hill equation was used to model the curing process for each of the samples. First, to better visualize the curing process, the curves shown in Figure 6a were normalized and plotted in Figure 7a. This graph represents the degree of conversion  $\alpha$  of the adhesive, which ranged from zero (at the beginning of curing) to one (when the adhesive was fully cured). As previously seen in Figure 6b, it is also clear in Figure 7a how increasing IPA content delayed the converging process. Figure 7b compares the experimental and theoretical curves of the baseline adhesive sample containing no IPA. The Hill model gives a good estimate of the curing kinetics of the adhesive.

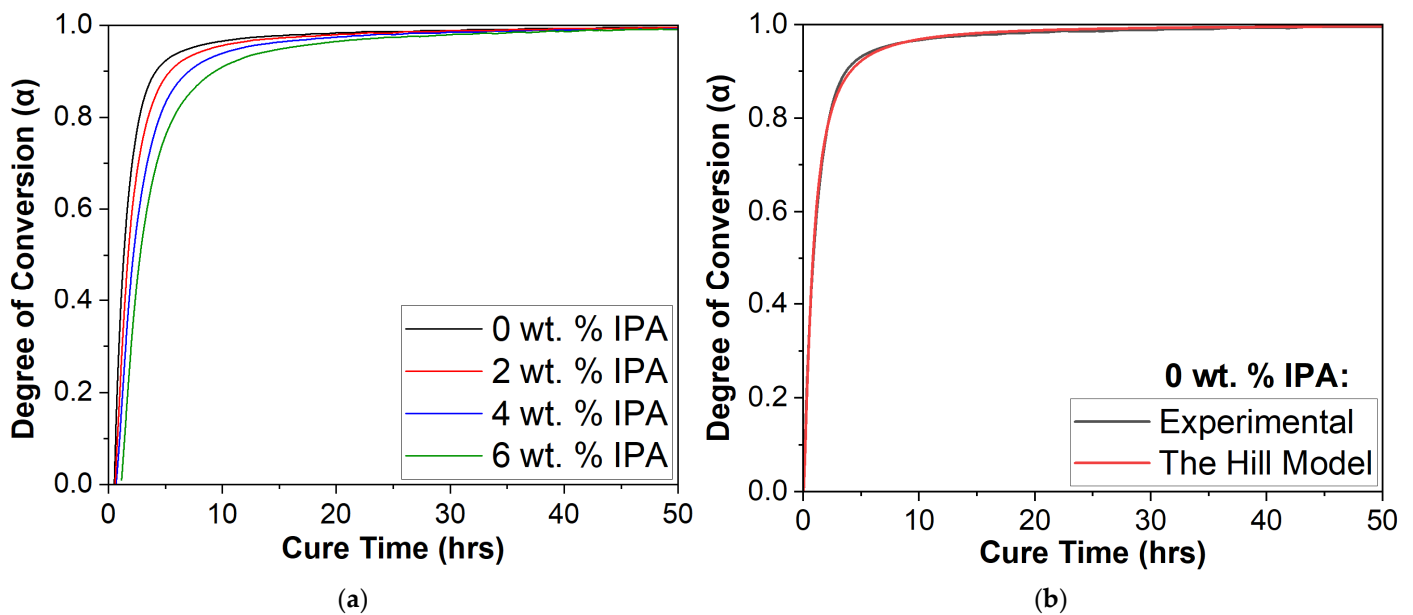


**Figure 7.** Degree of conversion with respect to cure time of (a) adhesive samples containing 0, 2, 4, and 6 wt.% of IPA; (b) experimental model using the Hill equation of the 0 wt.% IPA sample.

The values for the rate constant  $k$  and the shape parameter  $\theta$  obtained for each sample type after fitting the experimental data to the Hill equation using a GRG algorithm are summarized in Table 2. As expected, the rate constant decreased with increasing IPA content, although the decreasing rate decayed with increasing solvent content. On the other hand, the shape parameter for all the samples ranged between 1.35 to 1.48 and no particular trend was observed. The sum of errors (between the experimental and theoretical values) squared was small, meaning that the modeling resembled the experimental results.

### 3.6. Young's Modulus Using Ultrasonics vs. Tensile Testing

The density of the adhesive baseline sample was found to be  $1.113 \text{ g/cm}^3$ . This experimental value is slightly under the theoretical density of  $1.133 \text{ g/cm}^3$  obtained using the mass fractions of the resin and hardener components and their corresponding densities. This could have been caused by the presence of porosity introduced during the mixing process.

Figure 8 shows the longitudinal and shear time delays after performing the cross-correlation between the excitation and output signals versus the inverse of the frequency. Similarly to the method used by C. Pantea et al. [30], a total of five peaks of the cross-correlation were used: one corresponding to the overlap between the excitation; two to the left side of the overlap; and two to the right side of the overlap. After plotting and extrapolating the linear fits to a frequency of infinity, the intercept of each of the cycles where the inverse of the frequency equaled zero provided the sound travel time in the

sample. After taking into account the transducers and mold delay, the longitudinal travel time ranged from 4.881 to 4.951  $\mu\text{s}$ , which resulted in a sound speed of  $2271 \pm 18$  m/s. For the shear travel time, the time delay ranged from 11.240 to 11.293  $\mu\text{s}$ , which resulted in a sound speed of  $983 \pm 21$  m/s. Using these longitudinal and shear sound speeds in the adhesive, the Young's modulus and Poisson's ratio were calculated using Equations (3) and (4), respectively. The Young's modulus was determined to be  $2.963 \pm 0.133$  GPa, while the Poisson's ratio was calculated to be  $0.385 \pm 0.005$ .

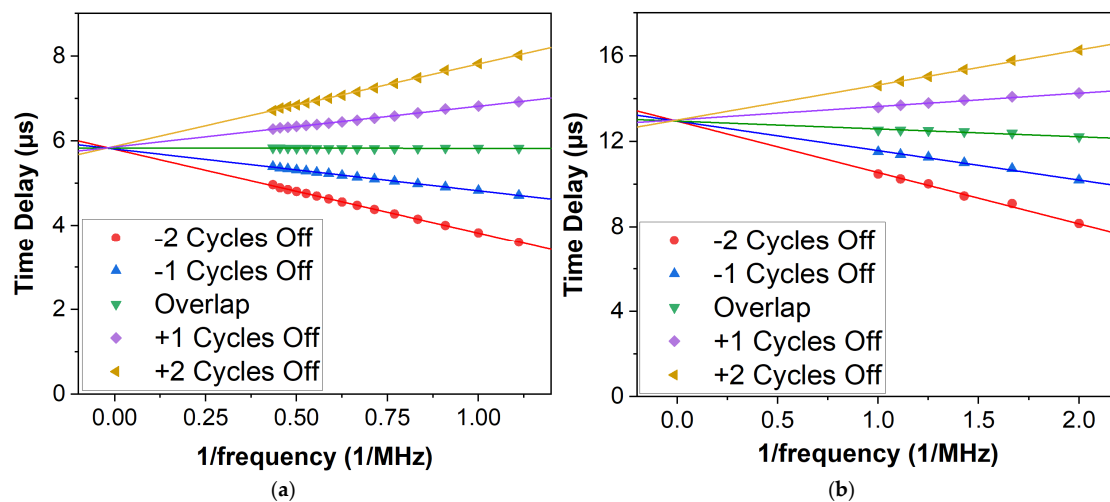


**Figure 8.** (a) Longitudinal time delay between the excitation and output signal vs.  $1/\text{frequency}$ ; (b) shear time delay between the excitation and output signal vs.  $1/\text{frequency}$ .

The average Young's modulus obtained using tensile testing was  $2.906 \pm 0.073$  GPa. This represents a difference of 1.92% with respect to the value determined using ultrasonics. This demonstrates the capability of ultrasonics as a non-destructive evaluation tool for measuring the elastic properties of an epoxy adhesive.

#### 4. Discussion

The presence of residual solvent in polymeric materials can considerably affect its curing process and chemical structure, thus altering its mechanical properties as well. In samples designed to observe this phenomenon, TGA confirmed that the presence of varying weight percentages of IPA in the adhesive affected its decomposition. Figure 2 shows how a higher wt.% of IPA caused higher weight loss from 100–320  $^{\circ}\text{C}$ , which is due to the IPA likely influencing the curing process of the adhesive [6,53]. This affected its chemical structure by possibly increasing the presence of lower molecular weight chains, which underwent thermal degradation earlier. FTIR also verified the presence of IPA within the structure of the adhesive which may have affected the crosslinking process during curing. Similar behavior was observed by M. Loos et al. when they investigated the effect of acetone on the properties of an epoxy resin [53].

Lap shear testing showed that the presence of trapped solvent in an adhesive can heavily decrease its adhesion properties. This is consistent with the results reported by C. Yi et al., in which they showed how the addition of 14 vol. % of xylene solvent into an epoxy adhesive decreased its adhesion strength by 35% [55]. They also reported that the samples with this same amount of solvent experienced a decrease of 60% in their tensile strength compared to the pristine resin samples. Figure 4b demonstrates that adhesive failure was obtained but no major visual changes in the failure surfaces occurred for the different sample types. This emphasizes the need for a non-destructive evaluation method, since performing destructive testing to obtain the properties of adhesives is time-consuming and costly. Ultrasonics can help in performing in situ testing during the manufacturing process,

and, as shown in Section 3.6, in obtaining the elastic properties of polymers if their density is known.

It was demonstrated that ultrasonics can be used to monitor the curing process of an epoxy adhesive by evaluating changes in sound speed due to variations in its chemical structure. The first test shown in Figure 5 of three different baseline adhesive samples shows that the ultrasonics setup could repeatedly be used to monitor the kinetics of polymer curing. This helped determine that the fluctuations in the curing behavior of the samples containing residual solvent (Figure 6) were due to the IPA preventing an ideal curing rate of the adhesive. Previous work has shown that the tensile strength of this adhesive with respect to cure time starts converging between curing hours 8 and 10 [56,57], meaning that the sound speed is more sensitive than tensile strength to the gelation process and early crosslinking between the polymer chains of the curing adhesive. Repeated laboratory testing reflected that both the mixing technique and the adhesive's temperature could influence its curing process. In addition, evaluating the sound speed in fully cured adhesives that are manufactured properly can serve as an in-field quality control method during the lifetime of those materials. The evaluation of the elastic properties of the epoxy adhesive using ultrasonics was corroborated with tensile testing values, validating this non-destructive evaluation method.

Modeling the curing process using the Hill equation helped in achieving a better numerical comprehension of how the curing rate of the adhesive was affected by the trapped solvent. This model can predict how improper manufacturing influences the properties of materials by correlating the rate constant  $k$  and shape parameter  $\theta$  to the strength of the polymer. A decreasing trend was observed for the rate constant although no variation was found for the shape parameter. Further analysis will be performed to correlate  $k$  and  $\theta$  to the types of chemical reactions occurring during the curing process and how those influence the final mechanical properties of the polymer, which, to the authors' knowledge, is a work that has yet to be performed. If a specific curing mechanism is associated with the final structure of the polymer, in situ analysis during the curing process could also determine if a part is safe or unsafe to use before waiting for the whole manufacturing process to be completed.

## 5. Conclusions

Solvents are commonly used during the manufacture of polymeric materials, which raises concerns about their proper removal. The influence of residual solvent on the curing process of an epoxy adhesive was studied. It was observed that the presence of IPA in the adhesive can have a significant impact on its physical and chemical properties. FTIR confirmed the presence of IPA within the polymer structure, while TGA showed that the solvent caused an increased and faster decomposition at lower temperatures. Catastrophic consequences can occur due to the considerable decrease in the adhesion properties of the epoxy, as revealed by the lap shear test. This suggests the need for the development of a non-destructive method for evaluating the curing process and viscoelastic properties of polymers. Ultrasonics have shown promising results for becoming a tool for polymer quality evaluation in both manufacturing and in-field settings.

**Author Contributions:** Methodology, B.B., C.P. and E.S.D.; validation, G.S., E.V., E.S., M.O. and D.M.; investigation, G.S. and E.V.; writing—original draft preparation, G.S.; writing—review and editing, T.R., E.S.D. and C.P.; project administration, B.B. and T.R. All authors have read and agreed to the published version of the manuscript.

**Funding:** The authors acknowledge the Partnership for Research and Education Consortium in Ceramics and Polymers (PRE-CCAP), formed via the Department of Energy grants (grant numbers DE-NA0003865 and DE-NA0004051). This research was also partially funded by the NSF PREM IMPAQT by providing student support (grant number 2122078).

**Institutional Review Board Statement:** Not applicable.

**Informed Consent Statement:** Not applicable.

**Data Availability Statement:** Not applicable.

**Acknowledgments:** The authors give special thanks to 3M for contributing the two-part epoxy adhesive for the project.

**Conflicts of Interest:** The authors declare no conflict of interest. The funders had no role in the design of the study; in the collection, analyses, or interpretation of data; in the writing of the manuscript; or in the decision to publish the results.

## References

1. Ahmad, O.A.; Al Kassasbeh, A.M.; Al Rawashdeh, M.A. Fabrication of Polymer Concrete of Light Weight and High Performance. *Int. J. GEOMATE* **2020**, *20*, 116–122. [[CrossRef](#)]
2. Cheng, G.; Sahli, M.; Gelin, J.C.; Barriere, T. Process parameter effects on dimensional accuracy of a hot embossing process for polymer-based micro-fluidic device manufacturing. *Int. J. Adv. Manuf. Technol.* **2014**, *75*, 225–235. [[CrossRef](#)]
3. Culbreath, C.J.; Gaerke, B.; Taylor, M.S.; McCullen, S.D.; Mefford, O.T. Effect of infill on resulting mechanical properties of additive manufactured bioresorbable polymers for medical devices. *Materialia* **2020**, *12*, 100732. [[CrossRef](#)]
4. Smirnov, A.V.; Genis, A.V. Effect of process parameters on the structure and physicochemical properties of nonwoven materials manufactured by aerodynamic spinning from polymer solution. *Fibre Chem.* **2002**, *34*, 24–29.
5. Sun, J.; Li, H.; Wang, H.; Yuan, D.; Stubbs, L.P.; He, C. The Effect of Residual Solvent N,N'-Dimethylformamide on the Curing Reaction and Mechanical Properties of Epoxy and Lignin Epoxy Composites. *Macromol. Chem. Phys.* **2016**, *217*, 1065–1073. [[CrossRef](#)]
6. Othman, N.H.; Mustapha, M.; Sallih, N.; Ahmad, A.; Mustapha, F.; Ismail, M.C. The Effect of Residual Solvent in Carbon-Based Filler Reinforced Polymer Coating on the Curing Properties, Mechanical and Corrosive Behaviour. *Materials* **2022**, *15*, 3445. [[CrossRef](#)]
7. Chowdhury, A.H.; Jafarizadeh, B.; Pala, N.; Wang, C. Wearable Capacitive Pressure Sensor for Contact and Non-Contact Sensing and Pulse Waveform Monitoring. *Molecules* **2022**, *27*, 6872. [[CrossRef](#)]
8. Kostina, J.; Bondarenko, G.; Gringolts, M.; Rodionov, A.; Rusakova, O.; Alentiev, A.; Yakimanskii, A.; Bogdanova, Y.; Gerasimov, V. Influence of residual solvent on physical and chemical properties of amorphous glassy polymer films. *Polym. Int.* **2013**, *62*, 1566–1574. [[CrossRef](#)]
9. Aurela, B.; Räisänen, T. Residual solvent content in heatset offset print. *J. High Resolut. Chromatogr.* **1993**, *16*, 422–424. [[CrossRef](#)]
10. Xue, G.; Peng, B.; Ye, T.; Wu, J.; Zhao, Y.; Liu, Y.; Yamada, H.; Chen, H.; Li, H. Effect of Aromatic Solvents Residuals on Electron Mobility of Organic Single Crystals. *Adv. Electron. Mater.* **2022**, *8*, 2200158. [[CrossRef](#)]
11. Grima, J.N.; Zerafa, C. On the effect of solvent molecules on the structure and mechanical properties of organic polyphenylacetylene auxetic re-entrant network polymers. *Phys. Status Solidi. B Basic Res.* **2013**, *250*, 2030–2037. [[CrossRef](#)]
12. Trinidad, J.; Chen, L.; Lian, A.; Zhao, B. Solvent Presence and its Impact on the Lap-Shear Strength of SDS-Decorated Graphene Hybrid Electrically Conductive Adhesives. *Int. J. Adhes. Adhes.* **2017**, *78*, 102–110. [[CrossRef](#)]
13. Qiu, K.; Tannenbaum, R.; Jacob, K.I. Effect of processing techniques and residual solvent on the thermal/mechanical properties of epoxy-cellulose nanocrystal nanocomposites. *Polym. Eng. Sci.* **2021**, *61*, 1281–1294. [[CrossRef](#)]
14. John, D.; Paul, T.; Orikasa, K.; Zhang, C.; Boesl, B.; Agarwal, A. Engineered Aluminum Powder Microstructure and Mechanical Properties by Heat Treatment for Optimized Cold Spray Deposition of High-Strength Coatings. *J. Therm. Spray Tech.* **2022**, *31*, 2537–2559. [[CrossRef](#)]
15. Denny, J.; Jinoop, A.N.; Paul, C.P.; Singh, R.; Bindra, K.S. Fatigue crack propagation behaviour of inconel 718 structures built using directed energy deposition based laser additive manufacturing. *Mater. Lett.* **2020**, *276*, 128241. [[CrossRef](#)]
16. Sukumaran, A.K.; Thampi, A.D.; Sneha, E.; Arif, M.; Rani, S.; Abdul, A.J. Effect of bovine serum albumin on the lubricant properties of rice bran oil: A biomimetic approach. *Sādhanā* **2021**, *46*, 207. [[CrossRef](#)]
17. Bacca, N.; Zhang, C.; Paul, T.; Sukumaran, A.K.; Denny, J.; Rengifo, S.; Park, C.; Chu, S.; Mazurkivich, M.; Scott, W.; et al. Tribological and neutron radiation properties of boron nitride nanotubes reinforced titanium composites under lunar environment. *J. Mater. Res.* **2022**, *37*, 4582–4593. [[CrossRef](#)]
18. Nautiyal, P.; Denis, N.; Dolmetsch, T.; Zhang, C.; Boesl, B.; Agarwal, A. Interface Engineering and Direct Observation of Strengthening Behavior in Field-Sintered Boron Nitride Nanotube–Magnesium Alloy Composite. *Adv. Eng. Mater.* **2020**, *22*, 2000170. [[CrossRef](#)]
19. Lou, L.; Paul, T.; Aguiar, B.A.; Dolmetsch, T.; Zhang, C.; Agarwal, A. Direct Observation of Adhesion and Mechanical Behavior of a Single Poly(lactic-co-glycolic acid) (PLGA) Fiber Using an In Situ Technique for Tissue Engineering. *Appl. Mater. Interfaces* **2022**, *14*, 42876–42886. [[CrossRef](#)] [[PubMed](#)]
20. Nisar, A.; Dolmetsch, T.; Paul, T.; Sakthivel, T.S.; Zhang, C.; Boesl, B.; Seal, S.; Agarwal, A. Unveiling enhanced oxidation resistance and mechanical integrity of multicomponent ultra-high temperature carbides. *J. Am. Ceram. Soc.* **2022**, *105*, 2500–2516. [[CrossRef](#)]
21. John, D.; Paul, T.; Sukumaran, A.K.; Seiseddos, G.; Boesl, B.; Agarwal, A. Profilometry-Based Indentation Plastometry for Evaluating Bulk Tensile Properties of Aluminum-Silicon Carbide Composites. *Adv. Eng. Mater.* **2023**, *2023*, 2201890. [[CrossRef](#)]

22. Maffezzoli, A.; Quarta, E.; Luprano, V.A.M.; Montagna, G.; Nicolais, L. Cure Monitoring of Epoxy Matrices for Composites by Ultrasonic Wave Propagation. *J. Appl. Polym. Sci.* **1969**, *73*, 1969–1977. [[CrossRef](#)]
23. Caluk, N.; Azizinamini, A. Introduction to the concept of modular blocks for lunar infrastructure. *Acta Astronaut.* **2023**, *207*, 153–166. [[CrossRef](#)]
24. Wu, R.; Zhang, H.; Yang, R.; Chen, W.; Chen, G. Nondestructive Testing for Corrosion Evaluation of Metal under Coating. *J. Sens.* **2021**, *2021*, 6640406. [[CrossRef](#)]
25. Liu, Y.; Tian, Q.; Guan, X. Grain size estimation using phased array ultrasound attenuation. *NDT E Int.* **2021**, *122*, 102479. [[CrossRef](#)]
26. Khedmatgozar Dolati, S.S.; Caluk, N.; Mehrabi, A.; Khedmatgozar Dolati, S.S. Non-Destructive Testing Applications for Steel Bridges. *Appl. Sci.* **2021**, *11*, 9757. [[CrossRef](#)]
27. Gyekenyesi, A. Techniques for monitoring damage in ceramic matrix composites. *J. Intell. Mater. Syst. Struct.* **2014**, *25*, 1531–1540. [[CrossRef](#)]
28. Wang, X.; Xie, H.; Tong, Y.; Wang, B.; Hu, H. Three-point bending properties of 3D\_C/C\_TiC\_Cu composites based on acoustic emission technology. *Mech. Syst. Signal Process.* **2023**, *184*, 109693. [[CrossRef](#)]
29. Matsukawa, M.; Nagai, I. Ultrasonic characterization of a polymerizing epoxy resin with imbalanced stoichiometry. *J. Acoust. Soc. Am.* **1996**, *99*, 2110. [[CrossRef](#)]
30. Pantea, C.; Rickel, D.G.; Migliori, A. Digital ultrasonic pulse-echo overlap system and algorithm for unambiguous determination of pulse transit time. *Rev. Sci. Instrum.* **2005**, *76*, 114902. [[CrossRef](#)]
31. Lionetto, F.; Maffezzoli, A. Monitoring the cure state of thermosetting resins by ultrasound. *Materials* **2013**, *6*, 3783–3804. [[CrossRef](#)] [[PubMed](#)]
32. Aggelis, D.G.; Paipetis, A.S. Monitoring of resin curing and hardening by ultrasound. *Constr. Build. Mater.* **2012**, *26*, 755–760. [[CrossRef](#)]
33. Shigang, A.; Rujie, H.; Yongmao, P. Effect of manufacturing defects on mechanical properties and failure features of 3D orthogonal woven C/C composites. *Composites* **2014**, *71*, 113–121. [[CrossRef](#)]
34. Soutis, C. Carbon fiber reinforced plastics in aircraft construction. *Mater. Sci. Eng.* **2005**, *412*, 171–176. [[CrossRef](#)]
35. Jayasree, N.A.; Airale, A.G.; Ferraris, A.; Messina, A.; Sisca, L.; Carello, M. Process analysis for structural optimisation of thermoplastic composite component using the building block approach. *Compos. B Eng.* **2017**, *126*, 119–132. [[CrossRef](#)]
36. Office of Aviation Research Washington. *Effects of Surface Preparation on the Long-Term Durability of Adhesively Bonded Composite Joints*; Office of Aviation Research Washington: Washington, DC, USA, 2004; DOT/FAA/AR-03/53.
37. Moutsompegka, E.; Tserpes, K.; Noeske, M.; Schlag, M.; Brune, K. Experimental Investigation of the Effect of Pre-Bond Contamination with Fingerprints and Ageing on the Fracture Toughness of Composite Bonded Joints. *Appl. Compos. Mater.* **2019**, *26*, 1001–1019. [[CrossRef](#)]
38. Drakonakis, V.M.; Seferis, J.C.; Doumanidis, C.C. Curing pressure influence of out-of-autoclave processing on structural composites for commercial aviation. *Adv. Mater. Sci. Eng.* **2013**, *2013*, 356824. [[CrossRef](#)]
39. Musaramthota, V.; Pribanic, T.; Mcdaniel, D.; Zhou, X. Effect of Surface Contamination on Composite Bond Integrity and Durability. *Joint Advanced Materials and Structures*; Baltimore, MD, USA, 2012.
40. Hernandez, B.; Gutierrez-Duran, G.; Dubon, J.; Pajon, M.; Rojas-Sanchez, J.F.; Boesl, B.; Mcdaniel, D. Effect of surface contamination with mitigation methods on adhesive composite bond integrity and durability. In Proceedings of the SAMPE, Charlotte, NC, USA, 20–23 May 2019.
41. Gupta, S.; Thorat, G.; Murthy, Z.V. Mixed Matrix PVA-GO-TiO<sub>2</sub> Membranes for the Dehydration of Isopropyl Alcohol by Pervaporation. *Macromol. Res.* **2020**, *28*, 587–595. [[CrossRef](#)]
42. Lua, Y.-Y.; Cao, X.; Rohrs, B.R.; Scott Aldrich, D. Surface Characterizations of Spin-Coated Films of Ethylcellulose and Hydroxypropyl Methylcellulose Blends. *Langmuir* **2007**, *23*, 4286–4292. [[CrossRef](#)]
43. Moiz, S.A.; Khan, I.A.; Younis, W.A.; Masud, M.I.; Ismail, Y.; Khawaja, Y.M. Solvent induced charge transport mechanism for conducting polymer at higher temperature. *Mater. Res. Express* **2020**, *7*, 095304. [[CrossRef](#)]
44. Kwon, J.T.; Moon, B.S.; Shin, J.K.; Lee, S.H.; Lee, S.H.; Lee, Y.S. A new polyfluorene containing repeated ethylenoxy units linked to glycerol as side chains: Synthesis and application as an electron injection material in the fabrication of polymer light-emitting diodes. *Synth. Met.* **2012**, *162*, 2163–2170. [[CrossRef](#)]
45. ASTM D5868-01; Standard Test Method for Lap Shear Adhesion for Fiber Reinforced Plastic (FRP) Bonding. ASTM International: West Conshohocken, PA, USA, 2004.
46. Joglekar, Y.N.; Wolf, S.J. SPICE model of memristive device using Tukey window function. *Circuits Syst. I* **2010**, *9*, 1–7. [[CrossRef](#)]
47. Stollenwerk, B.; Stock, S.; Siebert, U.; Lauterbach, K.W.; Holle, R. Uncertainty Assessment of Input Parameters for Economic Evaluation: Gauss's Error Propagation, an Alternative to Established Methods. *Med. Decis. Mak.* **2010**, *30*, 304–313. [[CrossRef](#)]
48. Focke, W.W.; van der Westhuizen, I.; Musee, N.; Loots, M.T. Kinetic interpretation of log-logistic dose-time response curves. *Sci. Rep.* **2017**, *7*, 2234. [[CrossRef](#)]
49. Lionetto, F.; Maffezzoli, A. Polymer Characterization by Ultrasonic Wave Propagation. *Adv. Polym. Technol.* **2008**, *27*, 63–73. [[CrossRef](#)]
50. Slotwinski, J.A.; Blessing, G.V. Ultrasonic Measurement of the Dynamic Elastic Moduli of Small Metal Samples. *J. Test. Eval.* **1999**, *27*, 164–166.

51. ASTM D638-03; Standard Test Method for Tensile Properties of Plastics. ASTM International: West Conshohocken, PA, USA, 2012.
52. Christensen, A.; Mashhadani, Z.T.A.W.; Abd Halim Bin Md Ali. In situ FTIR studies on the oxidation of isopropyl alcohol over SnO<sub>2</sub> as a function of temperature up to 600 °C and a comparison to the analogous plasma-driven process. *Phys. Chem. Chem. Phys.* **2018**, *20*, 9053–9062. [[CrossRef](#)]
53. Loos, M.R.; Coelho, L.A.F.; Pezzin, S.H.; Amico, S.C. The effect of acetone addition on the properties of epoxy. *Polimeros* **2008**, *18*, 76–80. [[CrossRef](#)]
54. Seisdedos, G.; Hernandez, B.; Dubon, J.; Ontiveros, M.; Boesl, B.; McDaniel, D. Non-Destructive Evaluation of Mechanical Damage of Adhesives Using Magneto-Electric Nanoparticles. *Am. Soc. Compos.* **2021**. [[CrossRef](#)]
55. Yi, C.; Rostron, P.; Vahdati, N.; Gunister, E.; Alfantazi, A. Curing kinetics and mechanical properties of epoxy based coatings: The influence of added solvent. *Prog. Org. Coat.* **2018**, *124*, 165–174. [[CrossRef](#)]
56. Dubon, J.; Seisdedos, G.; Watring, D.; Pajon, M.; Khizroev, S.; McDaniel, D.; Boesl, B. Multifunctional MEN-Doped Adhesives: Strengthening, Bond Quality Evaluation, and Variations in Magnetic Signal with Environmental Exposure. *Appl. Sci.* **2022**, *12*, 8238. [[CrossRef](#)]
57. Dubon, J.; Seisdedos, G.; Ontiveros, M.; Boesl, B.; McDaniel, D. Bond Quality Evaluation Using Adhesive Doped with Magneto-Electric Nanoparticles. *Am. Soc. Compos.* **2021**. [[CrossRef](#)]

**Disclaimer/Publisher’s Note:** The statements, opinions and data contained in all publications are solely those of the individual author(s) and contributor(s) and not of MDPI and/or the editor(s). MDPI and/or the editor(s) disclaim responsibility for any injury to people or property resulting from any ideas, methods, instructions or products referred to in the content.